


Article

Soft Computing Approach to Design a Triple-Band Slotted Microstrip Patch Antenna

Mahmud Esad Yiğit ^{1,2,*} , Gülay Öke Günel ³, Mustafa Emre Aydemir ⁴ and Tayfun Günel ⁵¹ Department of Electrical and Electronics Engineering, Çankırı Karatekin University, Çankırı 18100, Turkey² Graduate School, Department of Electronics & Communication Engineering, Istanbul Technical University, Istanbul 34469, Turkey³ Control and Automation Engineering Department, Istanbul Technical University, Istanbul 34469, Turkey⁴ Department of Electrical and Electronics Engineering, Istanbul Esenyurt University, Istanbul 34510, Turkey⁵ Department of Electronics & Communication Engineering, Istanbul Technical University, Istanbul 34469, Turkey

* Correspondence: eyigit@itu.edu.tr

Abstract: The design process of antenna structures that meet up-to-date requirements takes a long time and brings a high computational load. In this paper, an approach based on Soft Computing (SC) techniques was used to shorten the design time and to achieve an antenna structure that yields performance characteristics as close as possible to the desired values. In order to obtain a microstrip patch antenna with the targeted characteristics and the best accuracy in a faster way, a Support Vector Machine (SVM)-based regression model was employed. A triple-band microstrip antenna with desired resonance frequencies and gain values was designed by using the Support Vector Regression (SVR) model by introducing multiple slots and arc-truncation to the patch antenna. Simulation results of the High-Frequency Structural Simulator (HFSS) and measurements of implementation of the designed antenna are given. Performance characteristics of the obtained antenna are also compared with those given in the literature, which have triple-band properties. In addition, the antenna was redesigned using the optimization tool in HFSS for comparison. The accuracy of the results and required time for design were compared for both the SVR model approach and the HFSS optimization tool.

Keywords: microstrip patch antenna; slot antenna; soft computing; support vector machines; support vector regression; triple-band antenna



Citation: Yiğit, M.E.; Günel, G.Ö.; Aydemir, M.E.; Günel, T. Soft Computing Approach to Design a Triple-Band Slotted Microstrip Patch Antenna. *Appl. Sci.* **2022**, *12*, 11923. <https://doi.org/10.3390/app122311923>

Academic Editor: Daniele Funaro

Received: 10 October 2022

Accepted: 14 November 2022

Published: 22 November 2022

Publisher's Note: MDPI stays neutral with regard to jurisdictional claims in published maps and institutional affiliations.



Copyright: © 2022 by the authors. Licensee MDPI, Basel, Switzerland. This article is an open access article distributed under the terms and conditions of the Creative Commons Attribution (CC BY) license (<https://creativecommons.org/licenses/by/4.0/>).

1. Introduction

Soft computing (SC) refers to a group of methods that achieve tractable, robust, and low-cost solutions for problems that involve imprecise and uncertain conditions. Soft computing techniques are mainly inspired by intelligence in nature, such as the functioning principles of the biological brain, the reasoning mechanism of the human mind, or the natural selection principles of evolutionary processes. The term “Soft Computing” was proposed by Lotfi A. Zadeh [1,2].

The results obtained in SC techniques are not mathematically exact; approximate optimum results are obtained, whereas, in Hard Computing (HC), certain and precise results are attained. However, this increases computational time and load. In addition, HC requires the ideal model of the system or analytical expressions describing the behavior of the system and is not suitable for complex real-world problems where ideal model is not available. SC is the aggregation of various computational techniques. Some of the SC techniques and their applications include fuzzy logic [1,2], evolutionary algorithms [3–18], artificial neural networks (ANN) [19–27], and support vector machines (SVM) [19,20,28].

SVMs have been introduced by Vapnik [19,28]. Briefly, SVMs set up a hyperplane that separates two different sample sets from each other with a maximum margin in classification [20]. SVMs have usually been used for classification, but they are also used in

regression problems and are named Support Vector Regressors (SVR). SVRs have proven their capabilities in various studies of electromagnetics and microwaves due to their generalization properties [29–36]. They are used to design single-band antennas [32–36].

Electromagnetic simulation programs are used for antenna analysis and synthesis [37–39]. As the number of design parameters increases, the processing load and the time spent in the analyses performed by these programs also increase. Antennas need to be optimized with the changes in geometric structure to obtain the desired response. This also increases the design time. Even if the designer's knowledge and experience are sufficient, repetitively running programs with/without optimization or trial and error method negatively affects the design time. Furthermore, successful results are not guaranteed after repetitive trials.

Nowadays, there are many studies on the analysis and synthesis of microstrip antennas. Microstrip antennas have gained great interest since they were first introduced due to their features such as easy fabrication, low cost, compatibility with integrated circuits, and low weight. Moreover, by adding slots on the microstrip antenna patch and/or ground, antenna performance can be improved easily and efficiently. However, a general analytical formula for slots with various numbers and different types are not given in the literature so far. Additionally, the complexity of the design and time spent are increased with the number of slots.

In this paper, in order to overcome these drawbacks, a soft computing-based method is utilized in the design of a microstrip patch antenna that operates in triple-band. The resonance frequency and gain that yield the desired performance are obtained by utilizing an SVR model. Multiple slots and arc truncation [40,41] are implemented to patch the antenna to obtain an antenna that operates in triple-band with desired gains. The desired resonance frequencies of the triple-band are selected in 2.4 and 5 GHz bands of Wireless Local Area Network (WLAN) and the n80 (4.4–4.9 GHz) band [42] of 5G. There are two main novelties of the work presented, the first one is the novel structure of a triple-band antenna, and the second novelty is the implementation of a triple-band antenna designed using SVR for the first time. As far as the authors know, this work presents the first implementation of a triple-band antenna designed via SVR.

In order to verify the performance of the proposed antenna design method, simulation and implementation results are presented. Additionally, the achieved performance is compared with those of several antenna designs in the literature. The obtained results demonstrate the superiority of the proposed approach.

The contents of this paper are as follows: After this brief introduction, Section 2 presents a brief overview of Support Vector Regression. Section 3 describes the proposed design method for the triple-band antenna. Simulation and implementation results, as well as a comparison with existing designs in the technical literature, are presented in Section 4. Additionally, a comparison with the design carried out with the HFSS optimization tool is provided in Section 5. Section 6 briefly concludes the paper.

2. Theory of Support Vector Regression

A training data set S can be given by

$$S = \{x_i, y_i\}_{i=1}^N, x_i \in X \subseteq \mathbb{R}^n, y_i \in \mathbb{R} \quad (1)$$

where N is the number of elements in S and n is the dimension of the input. S can be represented by the regression model [20]:

$$y_i = \langle w, \Phi(x_i) \rangle + b \quad i = 1, 2, \dots, N \quad (2)$$

where $\Phi(x_i)$ is the image of the input data in feature space, b is regressor bias, and w is a weighting vector. The aim of the optimization is to find the optimal regressor within ε tube

by minimizing the training error and optimizing the geometric margin. The primal form of the optimization problem can be formulated as [20,43,44]:

$$\min_{(w,b)} \frac{1}{2} \|w\|^2 + C \sum_{i=1}^N (\xi_i + \xi_i^*) \quad (3)$$

subject to

$$\begin{aligned} y_i - \langle w, \Phi(x_i) \rangle - b &\leq \varepsilon + \xi_i \\ \langle w, \Phi(x_i) \rangle + b - y_i &\leq \varepsilon + \xi_i^* \\ \xi_i, \xi_i^* &\geq 0; \quad i = 1, 2, \dots, N \end{aligned} \quad (4)$$

where ε is the upper limit for the acceptable error, the slack variables ξ_i and ξ_i^* define the deviation from the ε tube [43,44]. The constraints of the optimization problem are constructed by an ε insensitive loss function [44,45]. The primal function and its constraints are used to define a Lagrange function. Lagrangian can be derived by combining the primal function and related constraints by presenting non-negative Lagrange multipliers β, β^*, η , and η^* [43,44]:

$$\begin{aligned} L = \frac{1}{2} \|w\|^2 + C \sum_{i=1}^N (\xi_i + \xi_i^*) - \sum_{i=1}^N \beta_i (\varepsilon + \xi_i - y_i + \langle w, \Phi(x_i) \rangle + b) - \sum_{i=1}^N \beta_i^* (\varepsilon + \xi_i^* + y_i - \langle w, \Phi(x_i) \rangle - b) \\ - \sum_{i=1}^N (\eta_i \xi_i + \eta_i^* \xi_i^*) \end{aligned} \quad (5)$$

Here, C is a parameter that controls the trade-off between the complexity of the obtained model and the number of non-separable points. For optimality, the partial derivatives of the Lagrangian with respect to primal variables have to vanish because of the saddle point property of the Lagrangian with respect to the primal variables and dual variables at the solution [44]:

$$\frac{\partial L}{\partial w} = 0 \rightarrow w - \sum_{i=1}^N \beta_i \langle w, \Phi(x_i) \rangle = 0 \quad (6)$$

$$\frac{\partial L}{\partial b} = 0 \rightarrow \sum_{i=1}^N (\beta_i - \beta_i^*) = 0 \quad (7)$$

$$\frac{\partial L}{\partial \xi_i} = 0 \rightarrow C - \beta_i - \eta_i = 0, \quad i = 1, 2, \dots, N \quad (8)$$

$$\frac{\partial L}{\partial \xi_i^*} = 0 \rightarrow C - \beta_i^* - \eta_i^* = 0, \quad i = 1, 2, \dots, N \quad (9)$$

The dual form can be defined by using optimality conditions (6–9) in (5):

$$D = \frac{1}{2} \sum_{i=1}^N \sum_{j=1}^N (\beta_i - \beta_i^*)(\beta_j - \beta_j^*) K_{ij} + \varepsilon \sum_{i=1}^N (\beta_i + \beta_i^*) - y_i \sum_{i=1}^N (\beta_i - \beta_i^*) \quad (10)$$

subject to

$$\begin{aligned} 0 &\leq \beta_i \leq C \\ 0 &\leq \beta_i^* \leq C \\ \sum_{i=1}^N (\beta_i - \beta_i^*) &= 0 \end{aligned} \quad i = 1, 2, \dots, N \quad (11)$$

where K_{ij} is the kernel function and can be given by $K_{ij} = \Phi^T(x_i)\Phi(x_j)$. The dual form has a convex objective function with linear constraints; therefore, a global solution to the problem is guaranteed. The optimal solution to the dual problem can be achieved by employing a quadratic programming solver, and the Lagrange multipliers are obtained.

The training data with non-zero Lagrange multipliers constitute the “support vectors” [43,45,46]. The regression problem of (2) can be solved by estimation via the support vectors and the corresponding Lagrange multipliers:

$$\hat{y}(x) = \sum_{i=1}^N \lambda_i K(\mathbf{x}, \mathbf{x}_i) + b, \quad \lambda_i = \beta_i - \beta_i^* \quad (12)$$

Mostly used kernel functions are linear, polynomial, and radial basis kernel (RBF) functions. RBF function can be given as:

$$K(\mathbf{X}_i, \mathbf{X}_j) = \exp(-\gamma \|\mathbf{X}_i - \mathbf{X}_j\|^2) \quad (13)$$

where γ is the Gaussian parameter and \mathbf{X} is the training vector.

Wavelet functions can also be used as kernel functions [47–50] in SVR, as well as the functions mentioned above. Wavelet analysis has the advantage that it processes signals in both time and frequency domains. The prediction is achieved more accurately via wavelet kernel than other types of kernel functions [35]. The orthonormality of wavelet functions results in an increase in the generalization capability of SVR [47]. A wavelet function is defined as [47]

$$h_{a,b}(x) = \frac{1}{\sqrt{a}} h\left(\frac{x-b}{a}\right) \quad (14)$$

where a is the scaling factor and b is the shifting parameter. Wavelet kernel is derived as [47]

$$K(\mathbf{X}, \mathbf{X}') = \prod_{i=1}^N h\left(\frac{x_i - b_i}{a}\right) h\left(\frac{x'_i - b'_i}{a}\right) \quad (15)$$

where \mathbf{X} and \mathbf{X}' are N -dimensional vectors, $h(x)$ is a wavelet function and $a, b_i, b'_i, x_i, x'_i \in \mathbb{R}$ and $\mathbf{X}, \mathbf{X}' \in \mathbb{R}^N$. Wavelet kernel independent of shifting is given as [47]:

$$K(\mathbf{X}, \mathbf{X}') = \prod_{i=1}^N h\left(\frac{x_i - x'_i}{a}\right) \quad (16)$$

The Morlet wavelet function is defined as [47,48]:

$$h(x) = \cos(1.75x) \exp\left(\frac{-x^2}{2}\right) \quad (17)$$

The Morlet wavelet kernel function is given as [47,48]:

$$K(\mathbf{X}, \mathbf{X}') = \prod_{i=1}^N \cos\left(1.75 \frac{(x_i - x'_i)}{a}\right) \cdot \exp\left(-\frac{\|x_i - x'_i\|}{2a^2}\right) \quad (18)$$

The Mexican-hat wavelet kernel function is written as [47,48]:

$$KK(\mathbf{X}, \mathbf{X}') = \prod_{i=1}^N \cos\left(1 - \frac{(x_i - x'_i)^2}{a}\right) \cdot \exp\left(-\frac{\|x_i - x'_i\|^2}{2a^2}\right) \quad (19)$$

In this study, wavelet kernel functions are preferred in the SVR approach due to their advantages, and specifically Mexican-hat wavelet kernel function is used since it has achieved the best results in the simulations. Other details related to the SVR design of the antenna are presented in the following sections.

3. Design of Triple-Band Antenna

Firstly, a rectangular microstrip patch antenna operating in 2.4 GHz of WLAN was designed by using formulations given in the literature [51].

The patch width (W) is computed by (20) for a rectangular microstrip patch antenna whose resonance frequency and relative permittivity of the substrate are f_r and ϵ_r , respectively [51]:

$$W = \frac{c}{2f_r} \sqrt{\frac{2}{\epsilon_r + 1}} \quad (20)$$

where c denotes the velocity of light in free space. The length of the antenna patch (L) can be calculated by [51]:

$$L = \left[\frac{c}{2f_r \sqrt{\epsilon_{eff}}} \right] - 2\Delta L \quad (21)$$

Here, ΔL is the extension of the length due to the effect of fringing fields and is given as [51]:

$$\Delta L = 0.412h \frac{(\epsilon_{eff} + 0.3) \left(\frac{W}{h} + 0.264 \right)}{(\epsilon_{eff} - 0.258) \left(\frac{W}{h} + 0.8 \right)} \quad (22)$$

Effective permittivity ϵ_{eff} is given by [51]:

$$\epsilon_{eff} = \left[\frac{\epsilon_r + 1}{2} \right] + \left[\frac{\epsilon_r - 1}{2} \right] \left[1 + \frac{12h}{W} \right]^{-1/2} \quad (23)$$

The desired resonance frequency of the rectangular microstrip patch antenna is selected as 2.4 GHz, WLAN base frequency. The antenna substrate is selected as Rogers RT/duroid 5870 with relative permittivity of 2.33, thickness of 0.787 mm, and loss tangent of 0.0012. By using (20–23), antenna patch dimensions L and W are computed as 38.6 mm and 47.5 mm, respectively. Then, parametric analysis in a High-Frequency Structural Simulator (HFSS) [37] is carried out to find the best reflection coefficient and input impedance and tune the resonance frequency to be close to 2.4 GHz for obtaining the feed location of the microstrip patch antenna without slots.

A parametric analysis method is used to simulate multiple variations for a design model [37]. A parametric analysis begins with the description of a series of variable values (variations) with chosen step sizes within a range. HFSS carries out an analysis of the design for each variation. Then, the results can be compared to see how each variation affects the performance of the design. Parametric analysis is frequently employed before the optimization process since it provides a reasonable range of variable values [37].

As a result of this process, the feed location of the antenna is computed as $x_f = 7.0$ mm and $y_f = 0$ mm. The same location is preserved for the microstrip patch antenna with triple slots and arc truncation.

After that, multiple slots were added to the conventional microstrip antenna that had the same patch dimensions and substrate to obtain multiband property. Then, the arc-truncation technique [40,41,52,53] was applied to the four edges of the antenna to improve gain performance. It is shown that there is an inverse relationship between the length of truncation and the Q factor of a truncated microstrip patch antenna [52,53]. Low radiation Q factor causes high antenna efficiency [52] value, which means high gain. In this study, it has also been observed that the reflection coefficient value decreases by introducing arc truncations to the antenna. This leads to an increase in the realized gain. The effect of the arc-truncation on the gain performance is ~ 1 dB increase. Center points for the two large slots are selected such that the slots are far away from the feed point and not so near to the edge of the antenna patch. The center point for the small slot is located at the upper half of the antenna patch. Thus, it is ensured that slots would not coincide with each other, feed point, and edges of the antenna. The initial positions of the slots were selected randomly. Then, parametric analysis via HFSS was carried out with a few steps to determine the positions of the slots, which provide frequency values close to the desired frequency bands. The geometric centers of the slots are equal to $x_1 = 0$ mm, $y_1 = -19.35$ mm; $x_2 = -7.32$ mm, $y_2 = 0$ mm; and $x_3 = 0$ mm, $y_3 = 19.35$ mm, respectively.

A general schematic representation of the microstrip patch antenna with triple slots and arc-truncation (MPATSAT) is shown in Figure 1a. L is the antenna length, W is the antenna width, $sL1$ and $sL2$ are the slot lengths, $sW1$ and $sW2$ are the slot widths, and r is the radius of the arc-truncation in Figure 1a. The sketch of MPATSAT in HFSS is also illustrated in Figure 1b.

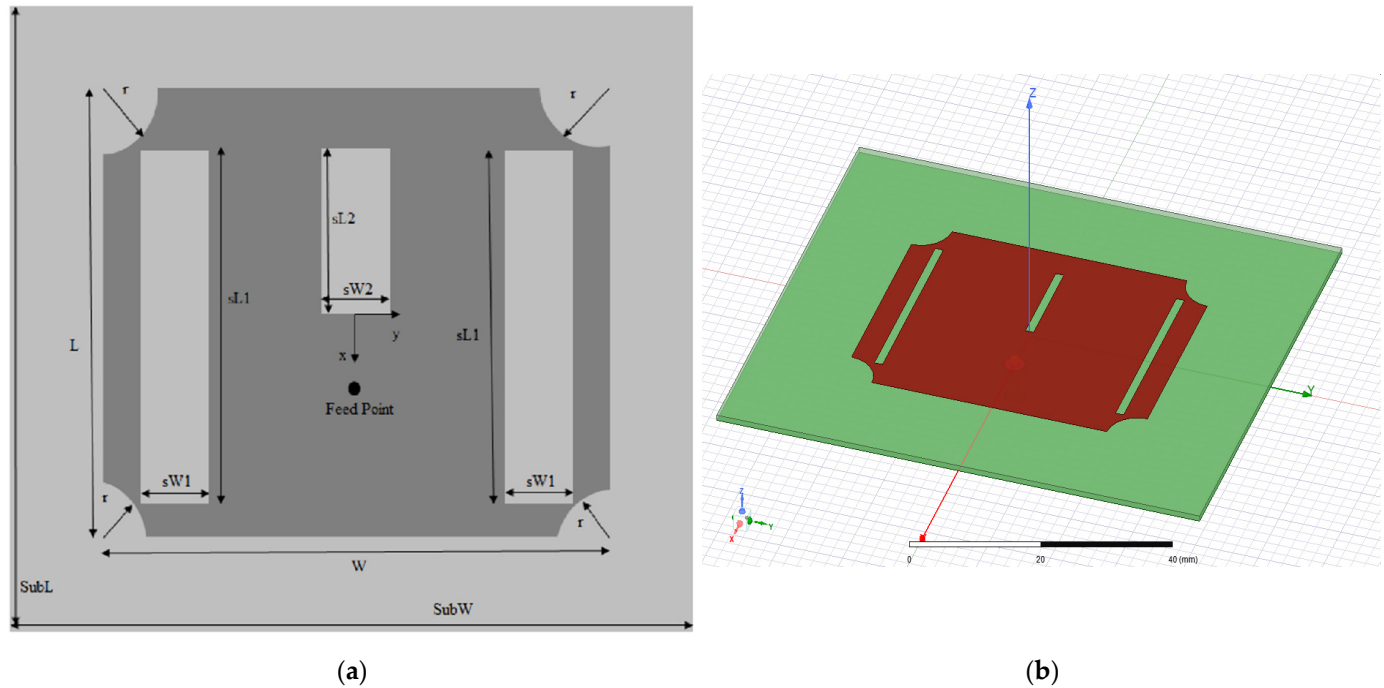


Figure 1. Drawings of the proposed antenna: (a) general schematic representation of MPATSAT; (b) sketch of MPATSAT in HFSS.

The inputs of the SVR model are triple-band resonance frequencies f_{r1} , f_{r2} , and f_{r3} and desired minimum gains at these frequencies g_1 , g_2 , and g_3 . The outputs of the SVR model are slot length and width values ($sL1$, $sL2$, $sW1$, and $sW2$) and the radius of arc-truncation (r) of the MPATSAT. The parametric analysis tool of HFSS was used to create proper training and testing patterns. Parametric analysis is used in HFSS to obtain resonance frequencies and gain values with respect to the slot dimensions and radii of arc-truncations. The sampling procedure for training and testing patterns is given in Table 1. Different values selected in an extensive range are used for constructing training and testing patterns to be able to obtain desired performance characteristics from the antenna. In soft computing methods, the selected dataset must cover all parts of the range that is required to be learned. The range of the slot dimensions and radii of the arc-truncations are selected to ensure that slots and truncation would not coincide with each other, feed point, and edges of the antenna. The step size between the selected samples of the ranges determines the number of samples. Step sizes are selected randomly; however, too-small values are avoided not to increase the computational load of the computer. The number of samples (variants) is limited by the computational power of the computer.

Table 1. Sampling procedure for training and testing.

Variables	Intervals and Number of Samples
slot Width 1 ($sW1$)	$0.5 \text{ mm} \leq sW1 \leq 10 \text{ mm}$
slot Width 2 ($sW2$)	$0.5 \text{ mm} \leq sW2 \leq 10 \text{ mm}$
slot Length 1 ($sL1$)	$10 \text{ mm} \leq sL1 \leq 30 \text{ mm}$
slot Length 2 ($sL2$)	$0.5 \text{ mm} \leq sL2 \leq 15 \text{ mm}$
radius of arc-truncation (r)	$0.5 \text{ mm} \leq r \leq 5 \text{ mm}$
number of training samples	1100
number of testing samples	149
total number of samples	1249

After parametric analysis, the whole HFFS' parametric analysis data are imported to MATLAB. Some of the elements of the data set are reserved as test samples, and the remaining ones are used to train the SVR model in MATLAB. Desired kernel function is selected and created in MATLAB via the required parameters (a for the Mexican-hat wavelet kernel). The dual form of the regression problem with linear constraints is written in MATLAB with related parameters (kernel function, C , ϵ). The dual form has a convex objective function with linear constraints; therefore, a global solution to the problem is guaranteed. The optimal solution of the dual problem can be achieved via employing a quadratic programming solver, and the Lagrange multipliers are obtained. "quadprog" function of MATLAB is used as a quadratic programming solver in this study. β and λ are obtained via a quadratic programming solver, and w values are updated. Bias (b) values are updated with respect to the difference between the output of the training pattern values and weight values. The regression problem of (2) is solved by obtaining λ , b and using the kernel function. In this way, a trained SVR model is obtained. This model can be used to compute the testing error, which gives the accuracy of the model. SVR model parameters related to the Mexican-hat wavelet kernel function are given in Table 2.

Table 2. SVR model parameters.

SVR Parameters	Selected Kernel Function Type and Parameter Values
Kernel function	Mexican-hat wavelet (19)
C	2×10^{12}
ϵ	5×10^{-4}
a	2.97

HFSS simulation of training and testing patterns with a total of 1249 samples took 2 h and 36 min using a computer that has 3.2 GHz CPU and 16 GB RAM. In total, 1100 training samples were used to train the SVR model, applying related parameters given in Table 2 via MATLAB [54]. The SVR parameters that yielded the best performance were selected. Training time was 2.8 s. Mean accuracy was acquired as 98.35% via testing with the remaining 149 test samples.

The trained SVR model was used to obtain geometric values of the MPATSAT ($sL1$, $sL2$, $sW1$, $sW2$, and r) for the desired resonant frequencies and desired minimum gains. Desired input resonance frequencies are chosen as $f_{r1} = 2.4 \text{ GHz}$, $f_{r2} = 4.7 \text{ GHz}$ and $f_{r3} = 5.3 \text{ GHz}$ bands for WLAN and 5G (n80) and expected minimum gain is $g = 5 \text{ dB}$. Geometric values of MPATSAT were computed as $sW1 = 1.3 \text{ mm}$, $sW2 = 0.65 \text{ mm}$, $sL1 = 29.3 \text{ mm}$, $sL2 = 14.70 \text{ mm}$, and $r = 4.9 \text{ mm}$ using the trained SVR model.

The design procedure is explained within a flow chart in Figure 2.

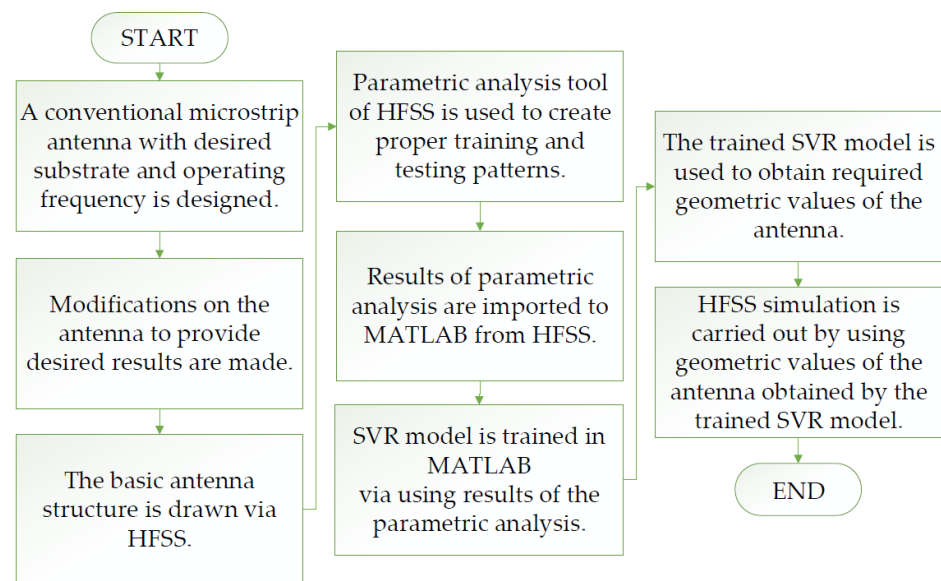


Figure 2. Flow chart of the design procedure.

4. Simulation and Implementation

HFSS simulation is carried out by using ($sL1$, $sL2$, $sW1$, and $sW2$) and (r) parameter values of the MPATSAT obtained by the trained SVR model in Section 3. $|S_{11}|$ plot of MPATSAT is illustrated in Figure 3. The obtained resonance frequencies are 2.45 GHz, 4.73 GHz, and 5.21 GHz. At these frequencies, the 10 dB bandwidths are obtained as 20 MHz, 40 MHz, and 50 MHz, respectively.

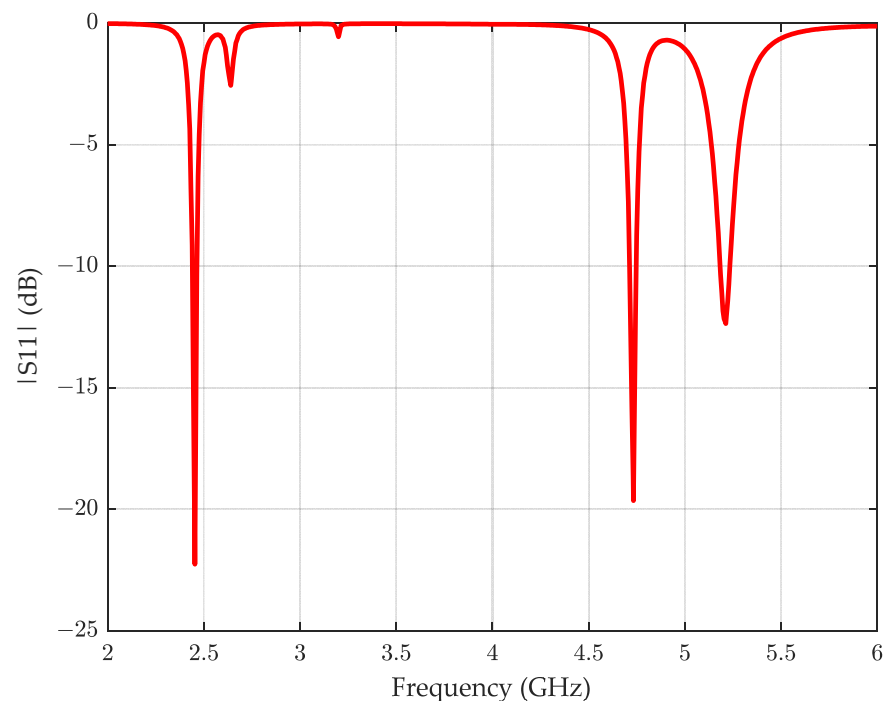


Figure 3. $|S_{11}|$ plot of MPATSAT.

Three-dimensional realized gain diagrams of MPATSAT for 2.45 GHz, 4.73 GHz, and 5.21 GHz are shown in Figure 4a–c, respectively. The maximum realized antenna gains are obtained as 6.1 dB, 4.6 dB, and 7.21 dB.

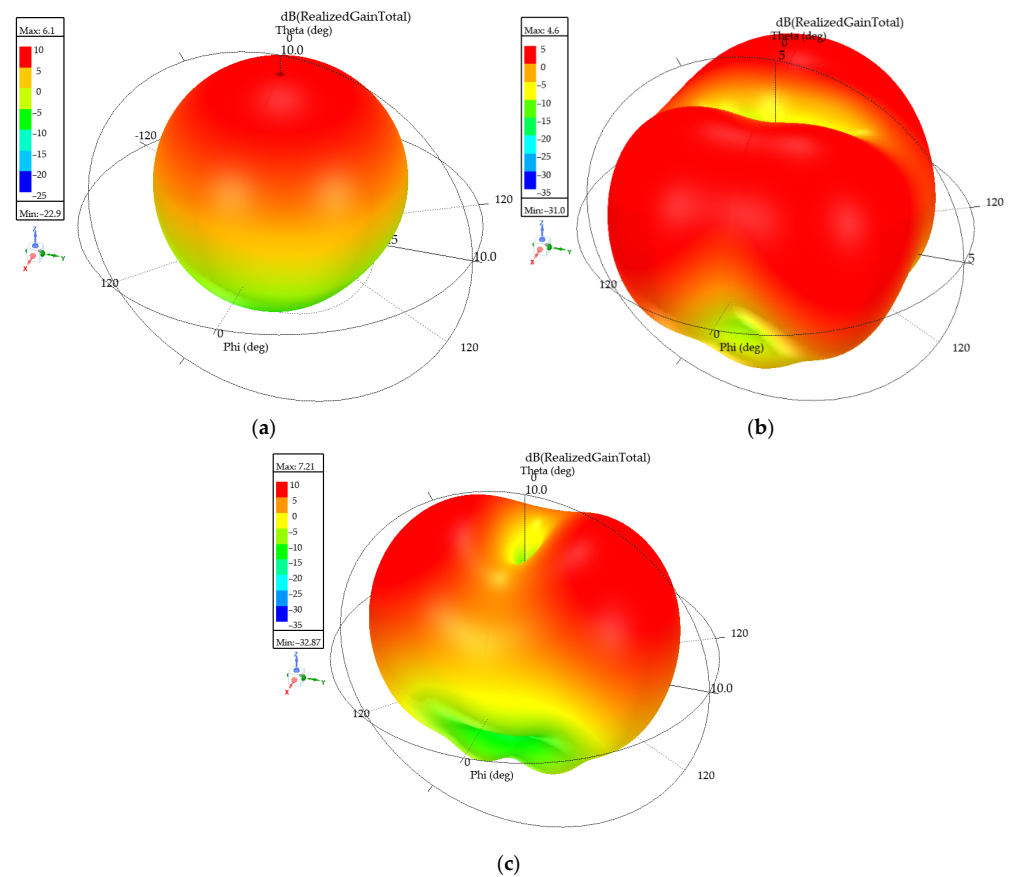


Figure 4. Three-dimensional realized gain diagrams of MPATSAT: (a) for 2.45 GHz; (b) for 4.73 GHz; (c) for 5.21 GHz.

$|Z_{11}|$ parameter plot of MPATSAT is given in Figure 5. Input impedances were tuned to $\sim 50 \Omega$ for resonance frequencies. Input impedances are 47.45Ω , 44.80Ω , and 47.02Ω for 2.45 GHz, 4.73 GHz, and 5.21 GHz, respectively.

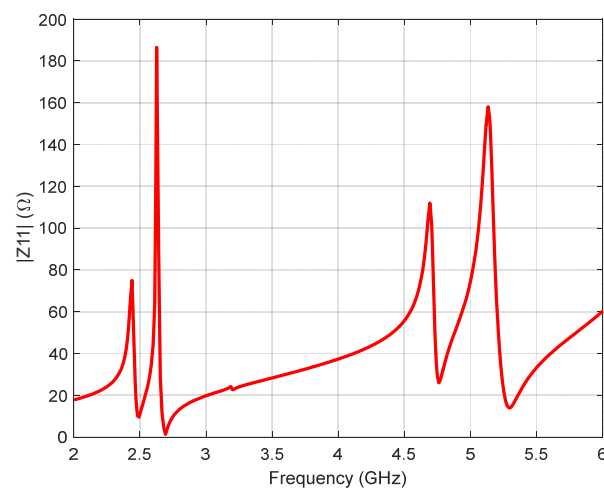


Figure 5. $|Z_{11}|$ plot of MPATSAT.

The co-polarization (co-pol.) and cross-polarization (cross-pol.) are very important from the application point of view to analyze the performance of antennas. In Figure 6a–c, co-pol. and cross-pol. radiation diagrams of MPATSAT are shown in the y–z plane and x–z plane for 2.45 GHz, 4.73 GHz, and 5.21 GHz, respectively.

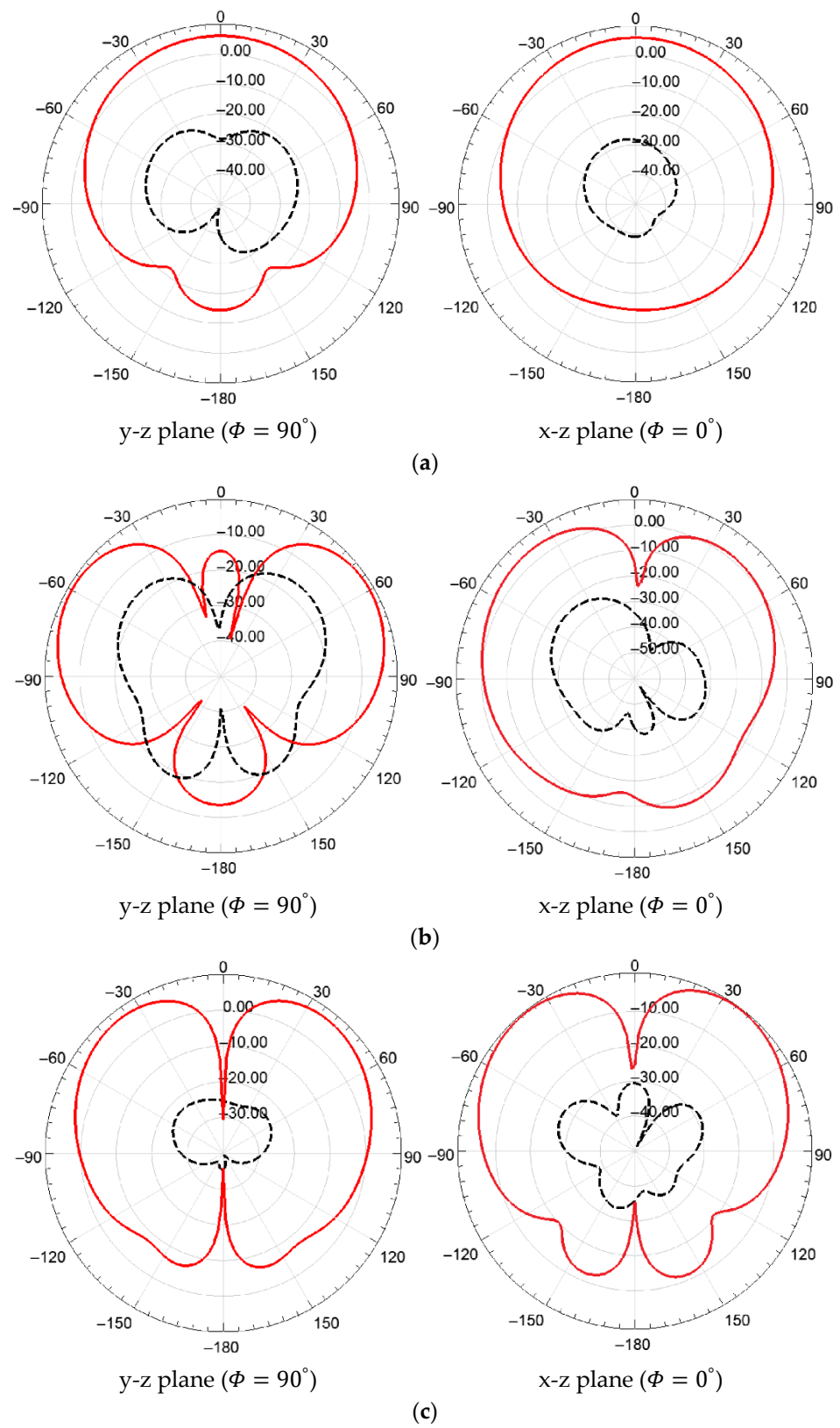


Figure 6. Co-pol. (—) and cross-pol. (---) radiation diagrams of MPATSAT in y-z ($\Phi = 90^\circ$) and x-z plane ($\Phi = 0^\circ$): (a) for 2.45 GHz; (b) for 4.73 GHz; (c) for 5.21 GHz.

Current distributions at the surface of MPATSAT for 2.45 GHz, 4.73 GHz, and 5.21 GHz are shown in Figure 7a–c, respectively. Current flows that cause the radiations in resonance frequencies can clearly be seen in Figure 7.

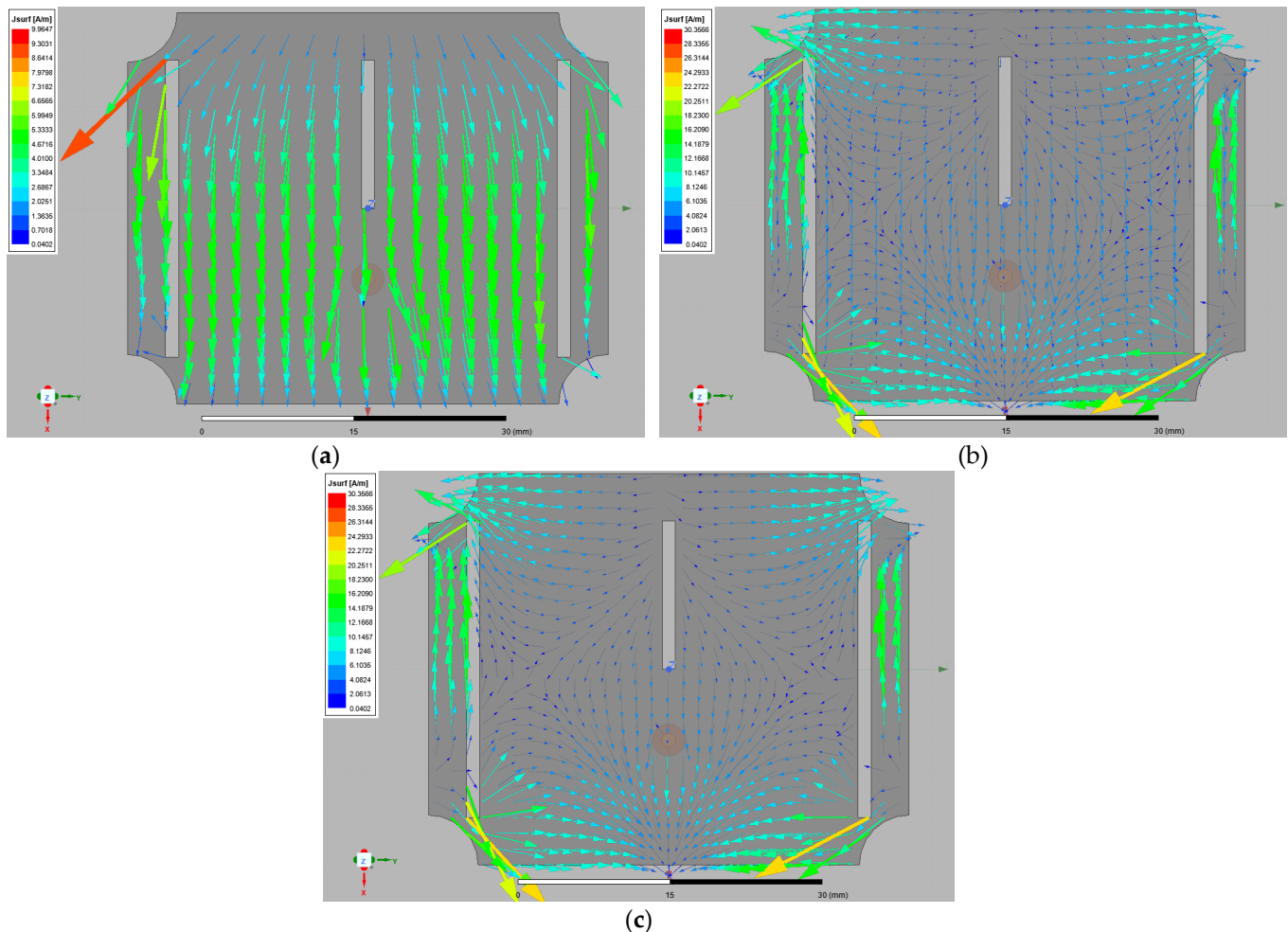


Figure 7. Current distributions at the surface of MPATSAT: (a) for 2.45 GHz; (b) for 4.73 GHz; (c) for 5.21 GHz.

Radiation efficiency is obtained as 96% for 2.45 GHz, 75% for 4.73 GHz, and 98% for 5.21 GHz. Satisfactory radiation efficiency values are acquired at the resonance frequencies.

MPATSAT given in Figure 1a,b was implemented by using Rogers RT/duroid 5870 with relative permittivity of 2.33 and substrate thickness of 0.787 mm and antenna geometric values given above. The top and bottom views of the implemented MPATSAT are presented in Figure 8a,b, respectively. The soldering in Figure 8 is implemented by hand in a classical way. After connections are tested via a Multimeter, no connection problem was detected between the outer conductor-antenna ground and inner conductor-antenna patch. $|S_{11}|$ plot of the implemented MPATSAT is obtained by a network analyzer.

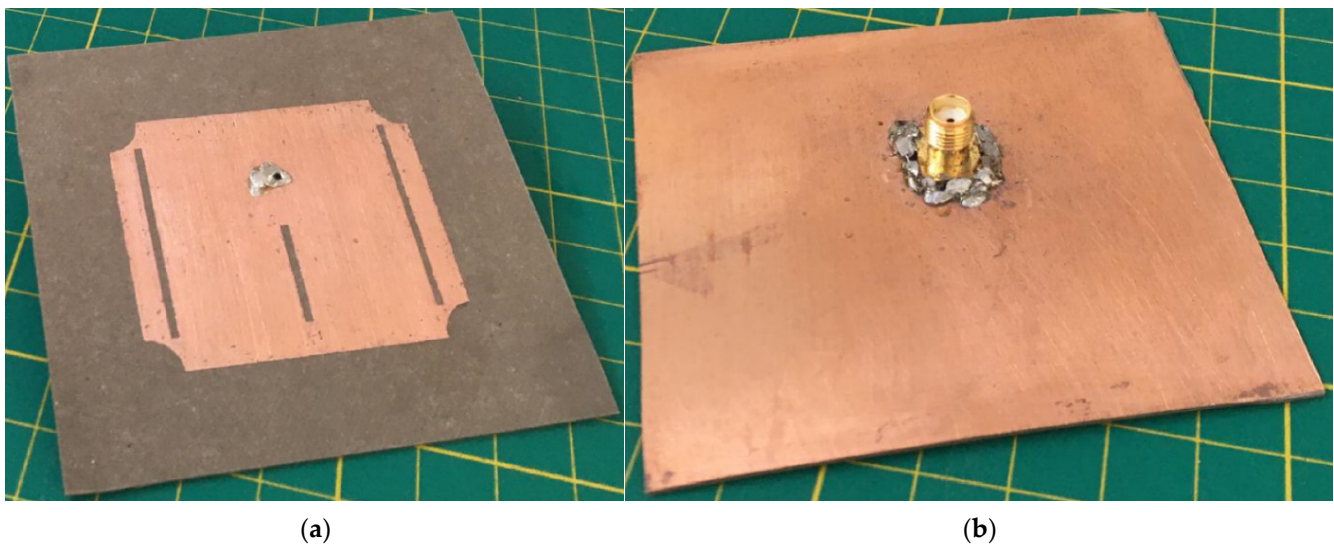


Figure 8. Implemented MPATSAT: (a) Top view; (b) Bottom view.

A comparison of $|S_{11}|$ plots of the simulation and measurement results is given in Figure 9. It can be observed that the simulation and measurement results coincide with each other approximately. The difference between simulation and measurement is due to measurement and implementation errors. The measured maximum antenna gains at the measured resonance frequencies are 3.1 dB, 3.8 dB, and 7.1 dB, respectively.

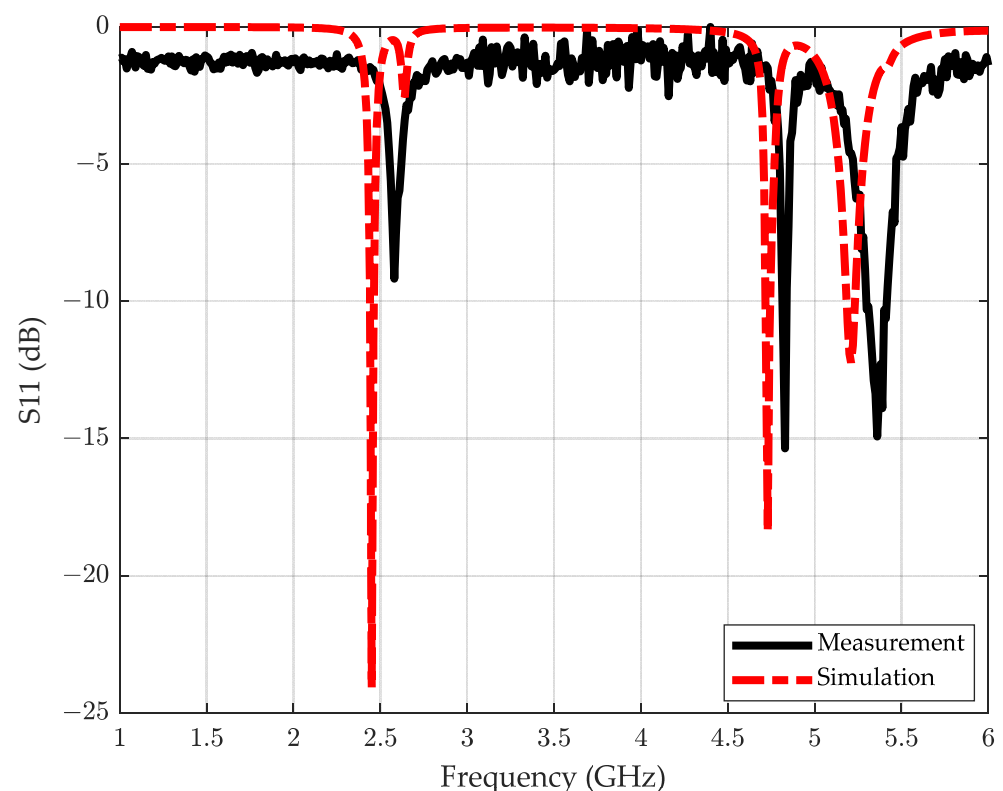


Figure 9. Comparison of $|S_{11}|$ plots of the simulation and the measurement.

Table 3 shows the comparison of the antenna designed by the proposed method with several triple-band antennas given in the literature [55–62]. In terms of antenna gains, MPATSAT gives relatively better results. It should be noted that these antennas given in the literature were not designed with soft computation techniques.

Table 3. Comparison of performance characteristics of MPATSAT with several antennas given in the literature.

	MPATSAT	[55]	[56]	[57]	[58]	[59]	[60]	[61]	[62]
number of bands	triple	triple	triple	triple	triple	triple	triple	triple	triple
antenna dimensions $L \times W$ (mm)	47.5×38.6	27 (radius)	34×18	20×21	29×10	60×60	40×50	60×60	44×45
substrate	RT Duroid 5870	RT Duroid 5870	FR-4	FR-4	FR-4	FR-4	FR-4	denim	FR-4
substrate thickness (mm)	0.787	1.5	1.6	1.57	1.6	1.56	0.8	1	1.6
resonance (operating) frequencies (GHz)	2.5	1.8	2.5	1.29	2.4	2.6	1.65	2.45	2.39
	4.8	2.4	3.5	2.44	3.5	4.2	1.93	3.25	3.55
	5.3	5.4	5.5	3.26	5.5	4.6	2.2	5.8	4.13
bandwidths (MHz)	20		300	210	80	580	70	76	196
	40	-	300	300	420	120	60	156	110
	50		1000	1390	600	100	280	328	220
gains at resonance frequencies (dB)	3.1	5.5	0.28	1.29	~1.75	4.4	1.08	0.025	4.05
	3.8	7.8	1.42	2.44	~2	3.9	1.82	−1.871	2.52
	7.1	7.9	4.76	3.26	~2.3	3.8	2.93	3.703	2.15

5. Antenna Design via HFSS Optimization Tool

In order to compare the results attained by the SVR method, the HFSS optimization tool was also used in this paper. The required time during the optimization and accuracy of the simulation results from the desired values are selected as the main comparison parameters. HFSS optimization tool includes various types of optimization methods such as gradient- and search-based algorithms.

In this study, Genetic Algorithm (GA) [3–8] and Pattern Search (PS) [63–65] methods were used as optimizer in the HFSS optimization setup. Goal parameters are selected as the magnitude of S11 in dB values at $f_{r1} = 2.4$ GHz, $f_{r2} = 4.7$ GHz, and $f_{r3} = 5.3$ GHz. Goal values are chosen to be less than or equal to -10 dB at these resonance frequencies. HFSS optimizer options are given in Table 4 for GA and PS. The same sampling strategy with the SVR model was used in the HFSS optimizer that is given in Table 1.

Table 4. HFSS optimizer options for Genetic Algorithm and Pattern Search.

Parameter	GA	PS
number of parents (current gen.)	30	-
number of mates	30	-
number of children	30	-
crossover type	simulated binary	-
mutation type	polynomial	-
number of survivors	10	-
number of individuals (next gen.)	30	-
selection type	roulette	-
selection pressure	10	-
maximum number of iterations	1000	1000
mutation probability	0.01	-
crossover probability	0.98	-
cost function norm type	L1	L1
weights	1	1

It can be observed that at the 715th iteration, the GA optimizer of HFSS obtained the optimal results. At the end of the optimization process via GA HFSS optimization tool, slot and arc truncation values are obtained as $sW1$ and $sW2 = 1.8$ mm, $sL1 = 25.5$ mm,

$sL2 = 12.75$ mm and $r = 1.36$ mm via HFSS optimization with GA optimizer. Resonance frequencies with these antenna geometric parameters are obtained as 2.37 GHz, 4.52 GHz, and 5.17 GHz by HFSS simulation. The maximum realized antenna gains are 5.9 dB, 3.5 dB, and 6.6 dB, respectively, for these resonance frequencies.

PS HFSS optimizer obtained the optimal results at the 625th iteration. Slot and arc truncation values are obtained as $sW1$ and $sW2 = 3.23$ mm, $sL1 = 21.34$ mm, $sL2 = 10.67$ mm, and $r = 1.0$ mm via HFSS optimization with PS optimizer. Resonance frequencies are obtained as 2.33 GHz, 4.54 GHz, and 5.38 GHz by HFSS simulation. The maximum realized antenna gains are 5.6 dB, 2.8 dB, and 6.5 dB, respectively, for the resonance frequencies.

Simulation results obtained by the SVR model approach given in Sections 3 and 4 were compared with the results obtained with HFSS optimizations; the comparison is provided in Table 5. Computation time for the SVR model is the required time for obtaining training and testing patterns via HFSS parametric simulation given in Section 3, and computation time for HFSS optimization is the total optimization time required by the HFSS optimization tool, as presented in Table 5. Computed resonance frequencies for the SVR model are given in Figure 3 of Section 4. Computed maximum realized gains at the resonance frequencies are given in Figure 4 of Section 4.

Table 5. Comparison of results of SVR model and HFSS optimization tool.

	SVR Model Approach	HFSS Optimization Tool (GA)	HFSS Optimization Tool (PS)
computation time	2 h and 36 min	9 h and 46 min	7 h and 32 min
TAE_f (GHz) (24)	0.17	0.34	0.31
desired resonance frequencies (GHz)	2.4 4.7 5.3	2.4 4.7 5.3	2.4 4.7 5.3
computed resonance frequencies (GHz)	2.45 4.73 5.21	2.37 4.52 5.17	2.33 4.54 5.38
computed maximum realized gains at the resonance frequencies (dB)	6.1 4.6 7.21	5.9 3.5 6.6	5.6 2.8 6.5

In Table 5, TAE denotes the total absolute error, and it is used to evaluate the accuracy of the methods used in this paper. TAE for resonance frequencies can be calculated by:

$$TAE_f = |f_{r1_d} - f_{r1_c}| + |f_{r2_d} - f_{r2_c}| + |f_{r3_d} - f_{r3_c}| \quad (24)$$

where f_{r1_d} , f_{r2_d} , and f_{r3_d} are the desired resonance frequencies; and f_{r1_c} , f_{r2_c} , and f_{r3_c} are the computed resonance frequencies.

6. Conclusions

In this paper, one of the soft computing methods, Support Vector Regression (SVR), was used to design a triple-band antenna with the desired resonance frequency and gain. The SVR model was utilized to obtain the optimal values for the geometric parameters of an antenna that provides the desired antenna variables. A microstrip patch antenna with triple slots and arc-truncation (MPATSAT) was simulated using these values via High-Frequency Structural Simulator (HFSS), and simulation and measurement results were compared. The performance characteristics of MPATSAT were compared with those obtained for several antennas given in the literature. Then, the antenna was redesigned by using the optimization tools in HFSS with the same desired antenna parameter values. The SVR approach and HFSS optimization method were compared with respect to accuracy and required computation time. These comparison results justify the superiority of the proposed design approach.

Author Contributions: Conceptualization, T.G. and M.E.Y.; methodology, T.G. and M.E.Y.; software, G.Ö.G. and M.E.Y.; validation, T.G., M.E.A. and M.E.Y.; investigation, M.E.Y. and M.E.A.; resources, T.G., G.Ö.G. and M.E.A.; writing—original draft preparation, M.E.Y.; writing—review and editing, G.Ö.G., T.G., M.E.A. and M.E.Y.; visualization, T.G. and M.E.Y.; supervision, T.G. All authors have read and agreed to the published version of the manuscript.

Funding: This research received no external funding.

Institutional Review Board Statement: Not applicable.

Informed Consent Statement: Not applicable.

Data Availability Statement: Not applicable.

Conflicts of Interest: The authors declare no conflict of interest.

References

1. Zadeh, L.A. Soft computing and fuzzy logic. *IEEE Softw.* **1994**, *11*, 48–56. [\[CrossRef\]](#)
2. Zadeh, L.A. Fuzzy logic = computing with words. *IEEE Trans. Fuzzy Syst.* **1996**, *4*, 103–111. [\[CrossRef\]](#)
3. Goldberg, D.E. *Genetic Algorithms in Search, Optimization and Machine Learning Reading*; Addison-Wesley: Boston, MA, USA, 1989.
4. Haupt, R.L. An introduction to genetic algorithms for electromagnetics. *IEEE Antennas Propag. Mag.* **1995**, *37*, 7–15. [\[CrossRef\]](#)
5. Weile, D.S.; Michielssen, E. Genetic algorithm optimization applied to electromagnetics: A review. *IEEE Trans. Antennas Propag.* **1997**, *45*, 343–353. [\[CrossRef\]](#)
6. Johnson, J.M.; Rahmat-Samii, V. Genetic algorithms in engineering electromagnetics. *IEEE Antennas Propag. Mag.* **1997**, *39*, 7–21. [\[CrossRef\]](#)
7. Haupt, R.L.; Werner, D.H. *Genetic Algorithm in Electromagnetics*; Wiley-Interscience: Hoboken, NJ, USA, 2007.
8. Haupt, R.L. Thinned arrays using genetic algorithms. *IEEE Trans. Antennas Propag.* **1994**, *42*, 993–999. [\[CrossRef\]](#)
9. Kennedy, J.; Eberhart, R. Particle swarm optimization. In Proceedings of the ICNN'95—International Conference on Neural Networks, Perth, WA, Australia, 27 November–1 December 1995. [\[CrossRef\]](#)
10. Robinson, J.; Rahmat-Samii, Y. Particle swarm optimization in electromagnetics. *IEEE Trans. Antennas Propag.* **2004**, *52*, 397–407. [\[CrossRef\]](#)
11. Boeringer, D.W.; Werner, D.H. Particle swarm optimization versus genetic algorithms for phased array synthesis. *IEEE Trans. Antennas Propag.* **2004**, *52*, 771–779. [\[CrossRef\]](#)
12. Taguchi, G.; Chowdury, S.; Wu, Y. *Taguchi's Quality Engineering Handbook*; Wiley-Interscience: Hoboken, NJ, USA, 2005.
13. Boyd, S.; Vandenberghe, L. *Convex Optimization*; Cambridge University Press: Cambridge, UK, 2004. Available online: https://web.stanford.edu/~boyd/cvxbook/bv_cvxbook.pdf (accessed on 8 October 2022).
14. Tsai, J.-T.; Liu, T.-K.; Chou, J.-H. Hybrid Taguchi-genetic algorithm for global numerical optimization. *IEEE Trans. Evol. Comput.* **2004**, *8*, 365–377. [\[CrossRef\]](#)
15. Afsari, A.; Abbosh, A.; Rahmat-Samii, Y. Adaptive beamforming by compact arrays using evolutionary optimization of Schelkunoff polynomials. *IEEE Trans. Antennas Propag.* **2022**, *70*, 4485–4497. [\[CrossRef\]](#)
16. Weng, W.; Yang, F.; Elsherbeni, A.Z. Linear antenna array synthesis using Taguchi's method: A novel optimization technique in electromagnetics. *IEEE Trans. Antennas Propag.* **2007**, *55*, 723–730. [\[CrossRef\]](#)
17. Günel, T.; Aydemir, E. Application of continuous parameter genetic algorithm to the problem of synthesizing bandpass distributed amplifiers. *AEU-Int. J. Electron. Commun.* **2002**, *56*, 351–354. [\[CrossRef\]](#)
18. Günel, T.; Yiğit, M.E.; Günel, G.Ö. Genetic-based approach to the synthesis of rectangular microstrip antenna elements with reduced mutual coupling. In Proceedings of the 2018 International Symposium on Advanced Electrical and Communication Technologies (ISAECT), Rabat, Morocco, 21–23 November 2018. [\[CrossRef\]](#)
19. Vapnik, V.N. An overview of statistical learning theory. *IEEE Trans. Neural Netw.* **1999**, *10*, 988–999. [\[CrossRef\]](#) [\[PubMed\]](#)
20. Haykin, S. *Neural Networks and Learning Machines*, 3rd ed.; Pearson Prentice Hall: Hoboken, NJ, USA, 2009.
21. Khan, T.; De, A. Modeling of microstrip antennas using neural networks techniques: A review. *Int. J. RF Microw. Comp. Aid. Eng.* **2015**, *25*, 747–757. [\[CrossRef\]](#)
22. Khan, T.; De, A. Prediction of slot-shape, slot-size and inserted air-gap of a microstrip antenna using knowledge-based neural network. *Prog. Electromagn. Res. C* **2016**, *65*, 23–32. [\[CrossRef\]](#)
23. Jain, S.K. Bandwidth enhancement of patch antennas using neural network dependent modified optimizer. *Int. J. Microw. Wirel. Technol.* **2016**, *8*, 1111–1119. [\[CrossRef\]](#)
24. Aneesh, M.; Singh, A.; Ansari, J.A.; Kamakshi; Sayeed, S.S. Investigations for performance improvement of X-shaped RMSA using artificial neural network by predicting slot size. *Prog. Electromagn. Res. C* **2014**, *47*, 55–63. [\[CrossRef\]](#)
25. Günel, T. Combination of artificial neural network model with genetic algorithm for the synthesis of microstrip radial stub. *AEU-Int. J. Electron. Commun.* **2000**, *54*, 241–243.
26. Aşık, U.; Günel, T.; Erer, I. A wavelet-based radial basis function neural network approach to the inverse scattering of conducting cylinders. *Microw. Opt. Technol. Lett.* **2004**, *41*, 506–510. [\[CrossRef\]](#)

27. Guney, K.; Sarikaya, N. A hybrid method based on combining artificial neural network and fuzzy inference system for simultaneous computation of resonant frequencies of rectangular, circular, and triangular microstrip antennas. *IEEE Trans. Antennas Propag.* **2007**, *55*, 659–668. [\[CrossRef\]](#)
28. Cortes, C.; Vapnik, V. Support vector network. *Mach. Learn.* **1995**, *20*, 273–297. [\[CrossRef\]](#)
29. Cai, J.; King, J.; Yu, C.; Liu, J.; Sun, L. Support vector regression-based behavioral modeling technique for RF power transistors. *IEEE Microw. Wirel. Compon. Lett.* **2018**, *28*, 428–430. [\[CrossRef\]](#)
30. Xu, J.; Jiang, W.; Ma, L.; Li, M.; Yu, Z.; Geng, Z. Augmented time-delay twin support vector regression-based behavioral modeling for digital predistortion of RF power amplifier. *IEEE Access* **2019**, *7*, 59832–59843. [\[CrossRef\]](#)
31. Wu, Y.; Tang, Z.; Xu, Y.; Guo, Y.; Zhang, B. Support vector regression for measuring electromagnetic parameters of magnetic thin-film materials. *IEEE Trans. Magn.* **2007**, *43*, 4071–4075. [\[CrossRef\]](#)
32. Angiulli, G.; Cacciola, M.; Versaci, M. Microwave devices and antennas modelling by support vector regression machines. In Proceedings of the 2006 12th Biennial IEEE Conference on Electromagnetic Field Computation, Miami, FL, USA, 30 April–3 May 2006. [\[CrossRef\]](#)
33. Tokan, N.T.; Gunes, F. Support vector design of the microstrip antenna. In Proceedings of the 2008 IEEE 16th Signal Processing, Communication and Applications Conference, Aydin, Turkey, 20–22 April 2008. [\[CrossRef\]](#)
34. Roy, C.; Khan, T.; Kanaujia, B. Performance parameters prediction of slotted microstrip antennas with modified ground plane using support vector machine. *Int. J. Microw. Wirel. Technol.* **2016**, *9*, 1169–1177. [\[CrossRef\]](#)
35. Yiğit, M.E.; Günel, T.; Günel, G.Ö. PSO based approach to the synthesis of a cylindrical-rectangular ring microstrip conformal antenna using SVR models with RBF and wavelet kernels. In Proceedings of the 2018 18th Mediterranean Microwave Symposium (MMS), Istanbul, Turkey, 31 October–2 November 2018. [\[CrossRef\]](#)
36. Dai, X.W.; Mi, D.L.; Wu, H.T.; Zhang, Y.H. Design of Compact Patch Antenna Based on Support Vector Regression. *Radioengineering* **2022**, *31*, 339–345. [\[CrossRef\]](#)
37. Ansys, HFSS 3D High Frequency Simulation Software. Available online: <https://www.ansys.com/products/electronics/ansys-hfss> (accessed on 8 October 2022).
38. Dassault Systems, CST Studio Suite Electromagnetic Field Simulation Software. Available online: <https://www.3ds.com/products-services/simulia/products/cst-studio-suite> (accessed on 8 October 2022).
39. Cadence, AWR Software Microwave Office. Available online: <https://www.awr.com/awr-software/products/microwave-office> (accessed on 8 October 2022).
40. Verma, S.; Ansari, J.A.; Singh, A. Truncated equilateral triangular microstrip antenna with and without superstrate. *Wirel. Pers. Commun.* **2017**, *95*, 873–889. [\[CrossRef\]](#)
41. Nirate, S.; Vani, R.M.; Hunagund, P.V.; Mallikarjun, S.L. Arc truncated suspended rectangular microstrip antenna. *Int. J. Adv. Res. Electr. Electron. Instrum. Eng.* **2016**, *5*, 1771–1775.
42. Kumar, S.; Dixit, A.S.; Malekar, R.R.; Raut, H.D.; Shevada, L.K. Fifth generation antennas: A comprehensive review of design and performance enhancement techniques. *IEEE Access* **2020**, *8*, 163568–163593. [\[CrossRef\]](#)
43. Iplikci, S. Online trained support vector machines-based generalized predictive control of non-linear systems. *Int. J. Adapt. Control. Signal Processing* **2006**, *20*, 599–621. [\[CrossRef\]](#)
44. Smola, A.J.; Schölkopf, B. A tutorial on support vector regression. *Stat. Comput.* **2004**, *14*, 199–222. [\[CrossRef\]](#)
45. Cristianini, N.; Shawe-Taylor, J. *An Introduction to Support Vector Machines and Other Kernel-Based Learning Methods*; Cambridge University Press: Cambridge, UK, 2000.
46. Iplikci, S. A comparative study on a novel model-based PID tuning and control mechanism for nonlinear systems. *Int. J. Robust Nonlinear Control* **2009**, *20*, 1483–1501. [\[CrossRef\]](#)
47. Hou, S.; Zhou, Y.; Liu, H.; Zhu, N. Wavelet support vector machine algorithm in power analysis attacks. *Radioengineering* **2017**, *26*, 890–902. [\[CrossRef\]](#)
48. Zhang, L.; Zhou, W.; Jiao, L. Wavelet support vector machine. *IEEE Trans. Syst. Man Cybern. Part B Cybern.* **2004**, *34*, 34–39. [\[CrossRef\]](#)
49. Parikh, U.B.; Das, B.; Maheshwari, R.P. Combined wavelet-SVM technique for fault zone detection in a series compensated transmission line. *IEEE Trans. Power Deliv.* **2008**, *23*, 1789–1794. [\[CrossRef\]](#)
50. Du, P.; Tan, K.; Xing, X. Wavelet SVM in reproducing kernel Hilbert space for hyperspectral remote sensing image classification. *Opt. Commun.* **2010**, *283*, 4978–4984. [\[CrossRef\]](#)
51. Balanis, C.A. *Antenna Theory Analysis and Design*, 3rd ed.; John Wiley & Sons, Inc.: Hoboken, NJ, USA, 2005.
52. Haneishi, M.; Yoshida, S. A design method of circularly polarized rectangular microstrip antenna by one-point feed. *Electron. Comm. Jpn. Part I* **1981**, *64*, 46–54. [\[CrossRef\]](#)
53. Mathew, S.; Anitha, R.; Deepak, U.; Aanandan, C.K.; Mohanan, P.; Vasudevan, K. A Compact tri-band dual-polarized corner-truncated sectoral patch antenna. *IEEE Trans. Antennas Propag.* **2015**, *63*, 5842–5845. [\[CrossRef\]](#)
54. Mathworks, MATLAB. Available online: <https://www.mathworks.com/products/matlab.html> (accessed on 9 September 2022).
55. Parveen, T.; Khan, Q.U.; Fazal, D.; Ali, U.; Akhtar, N. Design and analysis of triple band circular patch antenna. *AEU-Int. J. Electron. Commun.* **2019**, *112*, 152960. [\[CrossRef\]](#)
56. Li, Y.; Yu, W. A miniaturized triple band monopole antenna for WLAN and WIMAX applications. *Int. J. Antennas Propag.* **2015**, *2015*, 146780. [\[CrossRef\]](#)

-
57. Li, L.; Zhang, X.; Yin, X.; Zhou, L. A compact triple-band printed monopole antenna for WLAN/WiMAX applications. *IEEE Antennas Wirel. Propag. Lett.* **2016**, *15*, 1853–1855. [[CrossRef](#)]
 58. Zheng, Y.; Wang, P.; Hua, M.; Gao, P. Compact triple-band monopole antenna for WLAN/WiMAX applications. *IEICE Electron. Express* **2013**, *10*, 20130638. [[CrossRef](#)]
 59. Paul, P.M.; Kandasamy, K.K.; Sharawi, M.S. A tri-band slot antenna loaded with split ring resonators. *Microw. Opt. Technol. Lett.* **2017**, *59*, 2638–2643. [[CrossRef](#)]
 60. Sarkar, D.; Saurav, K.; Srivastava, K.V. Multi-band microstrip-fed slot antenna loaded with a split-ring resonator (SRR). *Electron. Lett.* **2014**, *50*, 1498–1500. [[CrossRef](#)]
 61. Li, H.; Du, J.; Yang, X.-X. Compact triple-band wearable circular patch antenna for WLAN/WiMAX applications. In Proceedings of the 2021 International Symposium on Antennas and Propagation (ISAP), Taipei, Taiwan, 19–22 October 2021. [[CrossRef](#)]
 62. Maity, B.; Nayak, S.K. Design of compact microstrip-fed triple-band slot antenna with defected ground structure for wireless communications. *J. Electromagn. Waves Appl.* **2022**, *36*, 1702–1716. [[CrossRef](#)]
 63. Hooke, R.; Jeeves, T.A. Direct search solution of numerical and statistical problems. *J. ACM* **1961**, *8*, 212–229. [[CrossRef](#)]
 64. Torczon, V. On the Convergence of pattern search algorithms. *SIAM J. Optim.* **1997**, *7*, 1–25. [[CrossRef](#)]
 65. Gardeux, V.; Omran, M.G.H.; Chelouah, R.; Siarry, P.; Glover, F. Adaptive pattern search for large-scale optimization. *Appl. Intell.* **2017**, *45*, 319–330. [[CrossRef](#)]